



# MIT Open Access Articles

## *Ionospheric Response to the Solar Eclipse of 21 August 2017 in Millstone Hill (42N) Observations*

The MIT Faculty has made this article openly available. **Please share** how this access benefits you. Your story matters.

|                     |  |
|---------------------|--|
| <b>Citation</b>     | Goncharenko, Larisa P., Erickson, Philip J., Zhang, Shun-Rong, Galkin, Ivan, Coster, Anthea J. et al. 2018. "Ionospheric Response to the Solar Eclipse of 21 August 2017 in Millstone Hill (42N) Observations." <i>Geophysical Research Letters</i> , 45 (10). |
| <b>As Published</b> | <a href="http://dx.doi.org/10.1029/2018gl077334">http://dx.doi.org/10.1029/2018gl077334</a>  |
| <b>Publisher</b>    | American Geophysical Union (AGU)   |
| <b>Version</b>      | Author's final manuscript  |
| <b>Citable link</b> | <a href="https://hdl.handle.net/1721.1/140471">https://hdl.handle.net/1721.1/140471</a>  |
| <b>Terms of Use</b> | Article is made available in accordance with the publisher's policy and may be subject to US copyright law. Please refer to the publisher's site for terms of use.   |

# Ionospheric Response to the Solar Eclipse of August 21, 2017 in Millstone Hill (42N) Observations

Larisa P. Goncharenko<sup>1</sup>, Philip J. Erickson<sup>1</sup>, Shun-Rong Zhang<sup>1</sup>, Ivan Galkin<sup>2</sup>, Anthea J. Coster<sup>1</sup>, Olusegun F. Jonah<sup>1</sup>

<sup>1</sup>Haystack Observatory, Massachusetts Institute of Technology, 99 Millstone Road, Westford, MA  
<sup>2</sup>University of Massachusetts in Lowell, 600 Suffolk St., Lowell, MA

## Key Points:

- Observations of ionospheric changes due to the Aug 21, 2017 solar eclipse
- Decrease in electron density by 30-40%, electron temperature by 100-220 K, ion temperature by 50-140 K
- Large 20-40 m/s vertical plasma drift seen in the topside ionosphere during recovery from eclipse is expected to affect plasmasphere

## Plain language summary

During the solar eclipse of August 21, 2017, millions of people who watched it from the ground could feel a sudden chill in the air as the moon's shadow moved across the continental US. However, it is far less certain what happens during the solar eclipse in the atmosphere at higher altitudes. Here we present ionospheric observations at 100-600 km above the ground and from > 1000 km away from the totality zone. We report up to 100-140 K cooling in the ion temperature which is very close to the temperature of neutral particles, 100-220 K cooling in electron temperature, and up to 40% reduction in electron density shortly after the maximum obscuration. We suggest that eclipse-induced ionospheric disturbances include a rapid upward flow of plasma from 200 km to much higher altitudes where the plasma is stored and then returned back to lower altitudes several hours after the end of the eclipse. We expect that such effects are stronger closer to the totality zone.

This is the author manuscript accepted for publication and has undergone full peer review but has not been through the copyediting, typesetting, pagination and proofreading process, which may lead to differences between this version and the [Version of Record](#). Please cite this article as doi: [10.1029/2018GL077334](https://doi.org/10.1029/2018GL077334)

Corresponding author: Larisa Goncharenko, [lpg@mit.edu](mailto:lpg@mit.edu)

## Abstract

This study examines the ionospheric changes associated with the solar eclipse of August 21, 2017. The effects associated with the passage of the eclipse shadow were observed more than 1000 km away from the totality at mid-latitudes using the Millstone Hill incoherent scatter radar and digisonde. There was a 30-40% decrease in electron density, a 100-220 K decrease in electron temperature, and a 50-140 K decrease in ion temperature. Surprisingly, the greatest decrease in electron density occurred above 200 km. The most unexpected effect was a large 20-40 m/s upward vertical drift observed in the topside ionosphere right after the local maximum obscuration. We suggest that this drift led to a post-eclipse increase in the topside electron density.

## 1 Introduction

Observations of ionospheric parameters during solar eclipses present a rare opportunity to examine our state of knowledge about fundamental processes responsible for ionospheric behavior. It is well known that the whole ionosphere, from the *E*, *F1*, and *F2* regions through the topside ionosphere, undergoes dramatic variations at eclipse times due to large changes in solar irradiation. Earlier studies of ionospheric response to solar eclipses consistently show a large decrease in electron density (50-60%) in the *E* and *F1* regions [Salah et al, 1986; Chernyak and Lysenko, 2013]. Changes in *NmE* and *NmF1* are directly proportional to the area of the Sun covered by the Moon [Le et al, 2008], as decreases in solar radiation lead to a decrease in electron production rates. However, *F2*-region ionospheric behavior can be much more complicated, resulting in either a decrease or even a small increase [Muller and Aylward, 1998] in electron density depending on background conditions and onset timing.

While observations of changes in electron density or total electron content during solar eclipses are more widely available in the modern era from networks of ionosondes and GNSS TEC receivers, direct observations of eclipse-induced variations in plasma temperatures and dynamics remain relatively rare. Incoherent scatter radars (ISRs) produce such direct observations due to the radar scattering dependence on plasma temperature, but only a handful of case studies have previously been available due to observational spatial coverage limitations. Evans [1965] reported that in observations with the Millstone Hill ISR during the afternoon eclipse of July 20, 1963, the electron temperature ( $T_e$ ) decreased by  $\sim 1000$  K, while the ion temperature ( $T_i$ ) decreased by 100 K at 350 km and 300 K at 650 km, closely following the solar extreme ultraviolet (EUV) obscuration function. Common ionospheric features reported in prior observations, in particular with ISR measurements, are a marked decrease in electron density (10-60%) and a 100 to 1000 K cooling in electron temperature. In general, the magnitude of ionospheric effects is to first order correlated with the level of EUV obscuration. However, even for a partial eclipse with obscuration of 0.42 under very low solar flux conditions ( $F_{10.7} = 66$  sfu), ISR eclipse observations have shown a decrease in electron temperature by 100-200 K and a decrease in F-region electron density by 25-30% [Domnin et al, 2013; Chernyak and Lysenko, 2013]. Observations of eclipse effects in the ion temperature are much less consistent, and range from reports of no measurable change [Chernyak and Lysenko, 2013] to a decrease of the order of 40-150 K [Domnin et al, 2013]. Eclipse-induced changes in the vertical drift range from no discernible effect at 200-300 km and  $\sim 20$  m/s downward drift at 400 km [Salah et al, 1986] to 10-45 m/s downward drift at all F-region altitudes [Domnin et al, 2013]. As changes in vertical drift result from the superposition of three sometimes equal processes - neutral wind forcing, electric field forcing, and ambipolar diffusion - the complicated patterns of observed ionospheric changes provide important condition-dependent information on the different roles of these processes.

This paper uses observations from the Millstone Hill incoherent scatter radar and a co-located digisonde (42.6°N, 288.5°E) to examine the impact of the August 21, 2017

77 solar eclipse on the mid-latitude ionosphere directly above the radar location. We focus  
78 only on low-frequency variations (on time scales  $> \sim 1.5$  hrs) that occur during the eclipse  
79 and for several hours after the end of the eclipse. Highlights of the results include a 30-  
80 40% decrease in the  $F2$ -region electron density, a relatively small 100-220 K decrease in  
81 electron temperature, and a strong upward drift above the  $F2$ -region peak following the  
82 eclipse.

## 83 2 Data and Methods

84 The Millstone Hill radar operated during August 19-23, 2017 and provided obser-  
85 vations prior to, during, and after the solar eclipse. The ISR operation mode was multi-  
86 purpose and included cycles alternating zenith pointing, fixed position pointing, and wide  
87 regional scans to the south (pointing towards the totality zone). From this comprehen-  
88 sive data set, we concentrate here on vertical ionospheric profiles. Height profiles of iono-  
89 spheric parameters were sampled with resolution of 4.5 km (best for the  $E$  and  $F1$ -region)  
90 and 18 km (best for the  $F2$ -region). The cycling radar mode described above resulted in  
91 vertical profile observations at irregular intervals every 7-15 mins. To accurately describe  
92 eclipse-induced changes and eliminate influences of TIDs that are omnipresent in observa-  
93 tions, we applied a temporal Savitzky-Golay smoothing filter [Savitsky and Golay, 1964]  
94 with a 2-degree (parabolic) polynomial over successive 2-hour subsets of data. We note  
95 that results remain essentially the same over a wide range of filter window lengths.

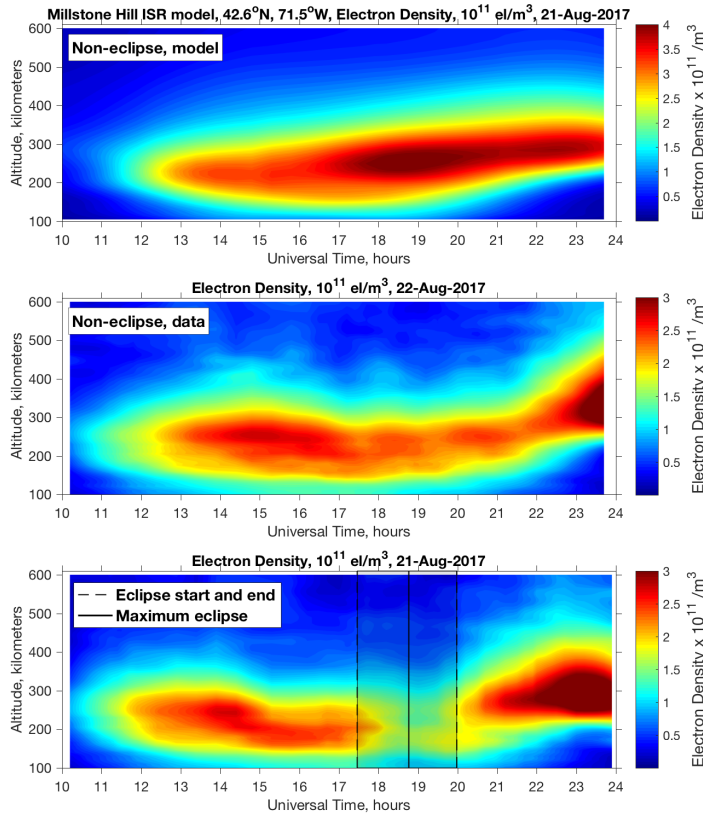
96 Observations by a co-located Millstone Hill digital ionosonde (digisonde) were con-  
97 tinuously available during the summer of 2017 with a high temporal resolution (1-2 mins),  
98 enabling further investigation of eclipse induced ionospheric changes in a manner comple-  
99 mentary to Millstone Hill ISR operations. A 5-min moving mean was applied to digisonde  
100 data to highlight essential ionospheric variations.

## 101 3 Geophysical conditions

102 The 21 August 2017 solar eclipse was visible in the continental US, and shadow  
103 passage started with a partial eclipse at 16:04 UT over Oregon, ending at 20:10 UT over  
104 South Carolina. At the Millstone Hill radar location, a partial solar eclipse was first ob-  
105 served at 17:27 UT (17.45 UT, 12.68 LT) and last observed at 19:59 UT (19.98 UT, 15.22  
106 LT). The maximum solar irradiation obscuration of 62.92% occurred at 18:46 UT (18.77  
107 UT, 14.00 LT), with a magnitude of 0.7. At the time of maximum obscuration over Mill-  
108 stone Hill, the center of totality was located at  $33^\circ\text{N}$  and  $80^\circ\text{W}$ , and therefore radar verti-  
109 cal profiles sampled the ionosphere directly above the site at a point more than 1000 km  
110 to the north-east from totality.

111 The eclipse occurred during low solar activity, with the solar flux ( $F10.7$ ) ranging  
112 from 86 to 91 SFU (1 SFU =  $1\text{E-}22$  W/m<sup>2</sup>/Hz) on August 19-23, 2017. This period also  
113 experienced minor to moderate geomagnetic activity, with maximum  $K_p = 4+$  to 5 on Au-  
114 gust 20,  $K_p = 3$  in the early hours of August 21,  $K_p = 4-$  to  $4+$  in the early hours of Au-  
115 gust 22, and  $K_p = 5-$  on August 19 and 23. Although several C class solar flares occurred  
116 on Aug 21 and 22, their influence was removed in our analysis through the Savitsky-Golay  
117 filtering described above.

118 In this study we have selected August 22, 2017 as the best available reference to  
119 represent the observed state of the non-eclipse ionosphere. To isolate eclipse effects, we  
120 also use predictions from the empirical incoherent scatter radar ionospheric model devel-  
121 oped from individual ISR long-term observations [Zhang and Holt, 2007].



123 **Figure 1.** Variations in electron density above Millstone Hill ISR (42.6°N, 288.5°E). (a) predicted by the  
 124 Millstone Hill empirical model for prevailing solar and geomagnetic conditions, (b) observed on a non-eclipse  
 125 day, August 22, 2017, and (c) observed during the eclipse on August 21, 2017.

## 122 4 Results

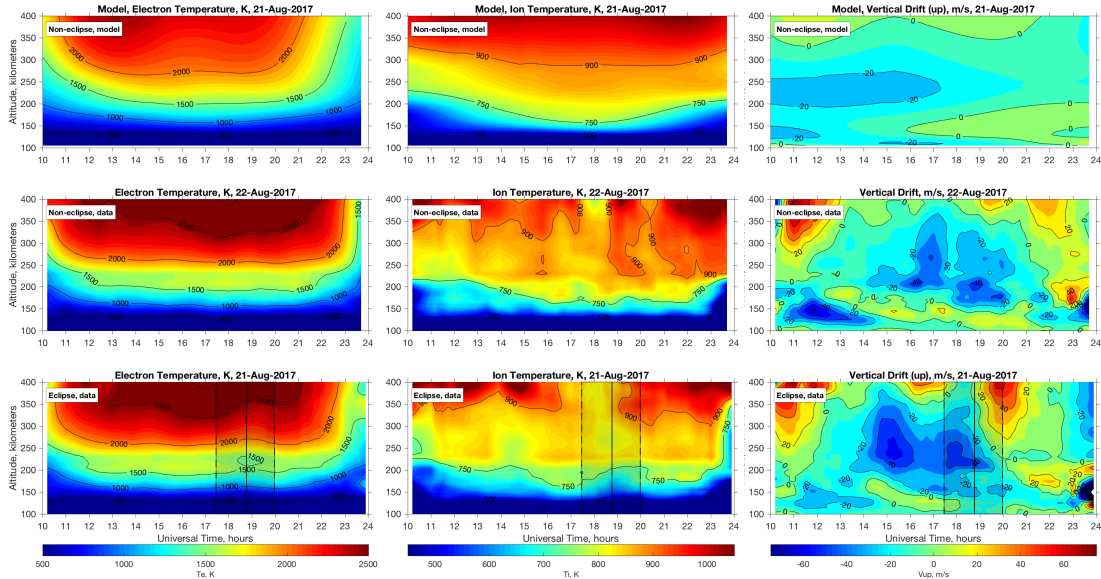
126 A summary of the mid-latitude electron density ( $N_e$ ) vertical observations over Mill-  
 127 stone Hill is presented in Figure 1. Figure 1a shows the electron density derived from the  
 128 Millstone Hill ISR empirical model for these solar and geomagnetic conditions. The main  
 129 features to note are a post-noon maximum in electron density between  $\sim 18$ -19 UTC and  
 130 a secondary maximum that occurs in the evening hours, between  $\sim 22$ -24 UTC. This is  
 131 typical well-known summer behavior that is associated with a combination of variations  
 132 in thermospheric wind, composition, and solar zenith angle. Figure 1b shows the obser-  
 133 vations on August 22, 2017, which was selected as the eclipse control (reference) day.  
 134 It demonstrates several differences from average behavior shown in Figure 1a. First, the  
 135 overall electron density was lower than the empirical model, likely due to the influence  
 136 of moderate geomagnetic activity that occurred in the early hours of August 22. Sec-  
 137 ond, the evening maximum was shifted toward later hours (23 to 02 UTC). The evening  
 138 peak in electron density was also observed at the same time, 23 to 02 UTC, during other  
 139 days of this campaign (August 19 and 20; not shown), and therefore it is possible that the  
 140 empirical model does not accurately represent the timing of the evening peak for these  
 141 conditions. Finally, Figure 1b also shows quasi-periodic fluctuations in  $N_e$  with scales of  
 142 the order of 2-3 hours that were superimposed on the smooth diurnal variation in  $N_e$ . To  
 143 summarize, the model and non-eclipse day observations predict that, in the absence of

144 eclipse effects, the *F2*-region electron density should have remained at steady levels or  
 145 somewhat increased in the afternoon hours (17 to 20 UT). Figure 1c shows observations  
 146 on the eclipse day, with the vertical lines indicating the start, maximum, and the end of  
 147 the partial eclipse over Millstone Hill. The main eclipse effect was a gradual decrease in  
 148 electron density at all altitudes from  $\sim 100$  km to  $\sim 600$  km, commencing soon after the  
 149 start of the partial eclipse. This was followed by a quick recovery after the eclipse shadow  
 150 passage at 20 UTC. The electron density response was altitude-dependent with altitudes  $<$   
 151  $200$  km recovering faster after the maximum eclipse than altitudes above  $\sim 250$  km, result-  
 152 ing in the peak electron density of the ionosphere being below  $200$  km. This is expected  
 153 due to rapid influences of photoionization rate changes on the photochemical equilibrium  
 154 at these heights.

155 Figure 2 presents variations in electron temperature (left), ion temperature (center)  
 156 and vertical plasma drift (right). The electron temperature on Aug 21 and 22 was gener-  
 157 ally higher than expected, likely due to the lower electron density lowering the elec-  
 158 tron cooling rate [Roble et al, 1986] and lower heat conduction from the plasmasphere.  
 159 The eclipse effect was clearly seen as a drop in  $T_e$  at  $200$ - $300$  km from  $\sim 1600$ - $1700$  K to  
 160  $\sim 1500$  K shortly after the time of maximum eclipse, at  $\sim 19$  UT. A decrease in ion  
 161 temperature was also observed around the time of maximum eclipse, though the magnitude  
 162 of this decrease was similar to other regularly occurring  $T_i$  variations (for example, at  $14$   
 163 to  $15$  UT). The vertical ion drift data reveals some unexpected behavior for summer solar  
 164 minimum conditions. At altitudes below  $200$  km, the vertical drift was dominated by  
 165 the presence of the semidiurnal tide in the lower thermospheric wind system, leading to  
 166 downward drift in the morning hours ( $11$ - $13$  UT) and upward drift later ( $15$ - $20$  UT). Local  
 167 sunrise at  $\sim 8.5$  UT (for  $250$  km) led to a rapid increase in plasma temperature that pro-  
 168 duced a strong upward drift above  $300$  km at  $10$ - $12$  UT. The daytime drift was generally  
 169 upward above  $350$  km, providing a flux of plasma into the plasmasphere, in consistency  
 170 with earlier observations [Evans, 1971]. All these features were stronger in observations  
 171 on August 21 and 22 than expected from the empirical model.

172 To highlight eclipse-related variations in electron density, Figure 3 shows differences  
 173 in electron density between August 21 and 22, 2017 in absolute (top) and relative percent-  
 174 age (bottom) units. The  $\sim 2$ - $3$  hr quasi-periodic variations on the control day (Figure 1b)  
 175 were removed by fitting to a smoothing spline that chosen to minimize edge effects. A de-  
 176 crease in electron density of  $0.5$ - $0.99 \times 10^{11}$   $\text{el}/\text{m}^3$  (30-40%) in the *F2*-region ( $200$ - $300$   
 177 km) is seen at the time of the eclipse, with the largest depletion  $\sim 8$ - $17$  mins after maxi-  
 178 mum obscuration. Below  $200$  km,  $N_e$  decreased by 10-20%. This  $N_e$  decrease diminished  
 179 at altitudes above  $300$  km. Above  $\sim 450$  km, eclipse-induced variations in general were  
 180 small and practically not discernible from the background which is subject to large day to  
 181 day changes. Another remarkable variation seen in Figure 3 was a quick recovery from  
 182 the eclipse and a large  $N_e$  increase that commenced soon after the eclipse, peaking at  $23$ -  
 183  $24$  UT. A similar post-eclipse increase above the background value was reported in several  
 184 studies of the August 21, 2017 solar eclipse over many locations across North America  
 185 [Nayak and Yiğit, 2017; Cherniak and Zakharenkova, 2018; Reinisch et al, 2018; Wu et  
 186 al, 2018], though the TEC increase is weaker in general as it reflects the integrated  $N_e$  re-  
 187 sponse over all altitudes. Mechanisms that contribute to a quick recovery and  $N_e$  increase  
 188 after 21 UT could include disturbances in the neutral wind and  $O/N_2$  ratio [Muller and  
 189 Aylward, 1998; Wu et al, 2018].

190 Eclipse induced changes in mid-latitude electron and ion temperatures and vertical  
 191 plasma velocity are shown in Figure 4. The electron temperature decreased by  $100$ - $220$   
 192 K during the eclipse, with the coldest temperatures being observed with a  $10$ - $20$  min-  
 193 utes time lag after the maximum obscuration near the *F2*-region peak ( $\sim 220$  km) and with  
 194  $\sim 20$ - $30$  minutes time lag at  $350$  km. A sharp reduction in the electron temperature might  
 195 be expected due to the decrease in photoelectron heating associated with the reduction in  
 196 EUV photoionization and the reduction in  $N_e$ , which linearly reduces the photoelectron  
 197

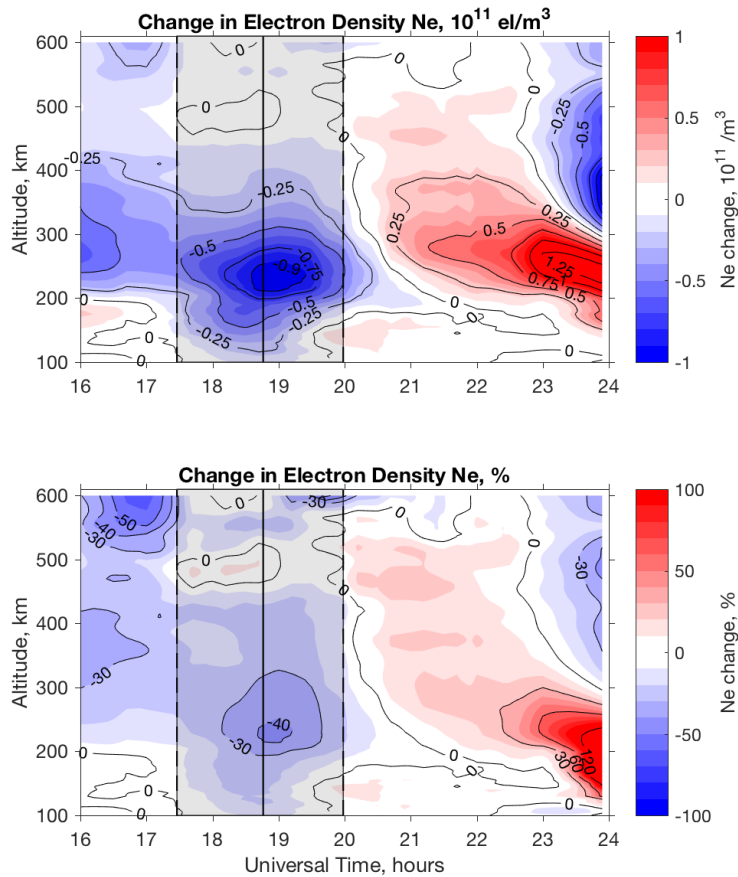


172 **Figure 2.** Variations in electron temperature, ion temperature, and vertical drift (positive upward) above  
 173 Millstone Hill ISR as (top) predicted by the Millstone Hill empirical model, (middle) observed on a non-  
 174 eclipse day, August 22, 2017, and (bottom) observed during the eclipse on August 21, 2017.

204 heating. On the other hand, the effect of the decreased heating is opposed by the reduction  
 205 in thermal electron cooling, which is quadratic in  $N_e$ . Enhanced downward heat flow from  
 206 the plasmasphere can also contribute to reduced temperature variations. The magnitude of  
 207 the 2017 eclipse temperature reduction was much smaller than reported in other eclipse  
 208 cases at middle latitudes. Earlier studies reported a larger 500-700 K decrease in elec-  
 209 tron temperature above Millstone Hill for an eclipse with a larger maximum obscuration  
 210 of 86% [Salah et al, 1986], and even 1000 K decrease for an eclipse with 100% obscura-  
 211 tion [Evans, 1965]. It is likely that the large decreases in electron temperature reported for  
 212 these cases are actually related to the sunset in the conjugate ionosphere.

213 The 2017 eclipse caused a maximum 70-80 K drop in ion temperature between 250-  
 214 300 km, centered around the time of maximum obscuration, and a 100-140 K drop in ion  
 215 temperature at altitudes 150-200 km that lagged behind the time of maximum obscuration.  
 216 The reduction in ion temperature likely resulted from thermospheric cooling due to the  
 217 passage of the eclipse shadow and from smaller Coulomb inelastic heat transfer from elec-  
 218 trons. A major 100-200 K drop in ion temperature was also observed after the eclipse at  
 219 23-24 UT, at the time of a large increase in electron density.

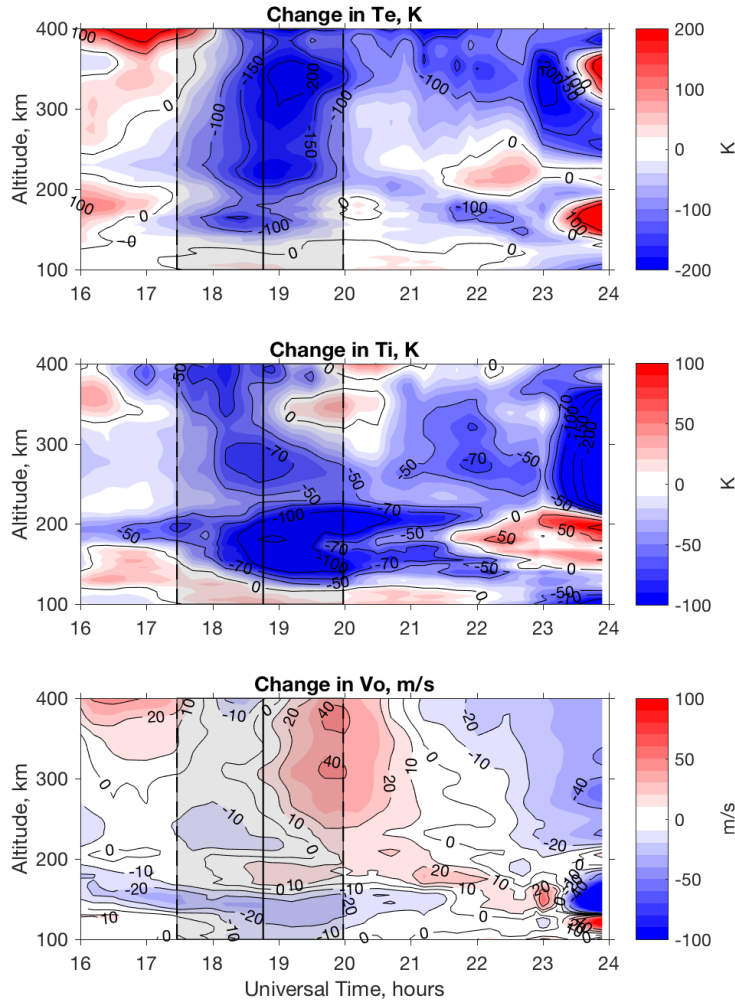
220 Vertical plasma drift ( $O^+$  velocity) during the daytime was generally weakly posi-  
 221 tive (upward) above  $\sim 350$  km with magnitudes of 0-15 m/s and negative (downward) at  
 222 0-15 m/s between 200-350 km altitude, as seen in Figure 2, in consistency with empiri-  
 223 cal model and earlier studies [Evans, 1971]. During the eclipse, Figure 4 shows that a  
 224 10-15 m/s stronger downward drift was observed between 200-270 km immediately af-  
 225 ter the start of the eclipse, while there were no measurable changes at higher altitudes. A  
 226 very strong upward plasma motion with speeds up to 40 m/s higher than normal was ob-  
 227 served for  $\sim 2$  hours after the maximum eclipse (19-21 UTC). The aggregate changes are  
 228 reminiscent of the effects of a local sunrise, and drift velocities are comparable to veloc-  
 229 ities observed after the sunrise (see Figure 2). This upward motion could be potentially  
 230 caused by two contributing factors: (1) immediate (at supersonic speed) ionospheric and  
 231 thermospheric heating due to recovery from the eclipse, and (2) enhanced southward and



193 **Figure 3.** Difference in electron density observed on the eclipse day, August 21, 2017, in comparison with  
 194 August 22, 2017.

232 eastward (directed towards maximum shadow) wind as would be anticipated in the eclipse-  
 233 induced colder thermosphere [Harding et al, 2018].

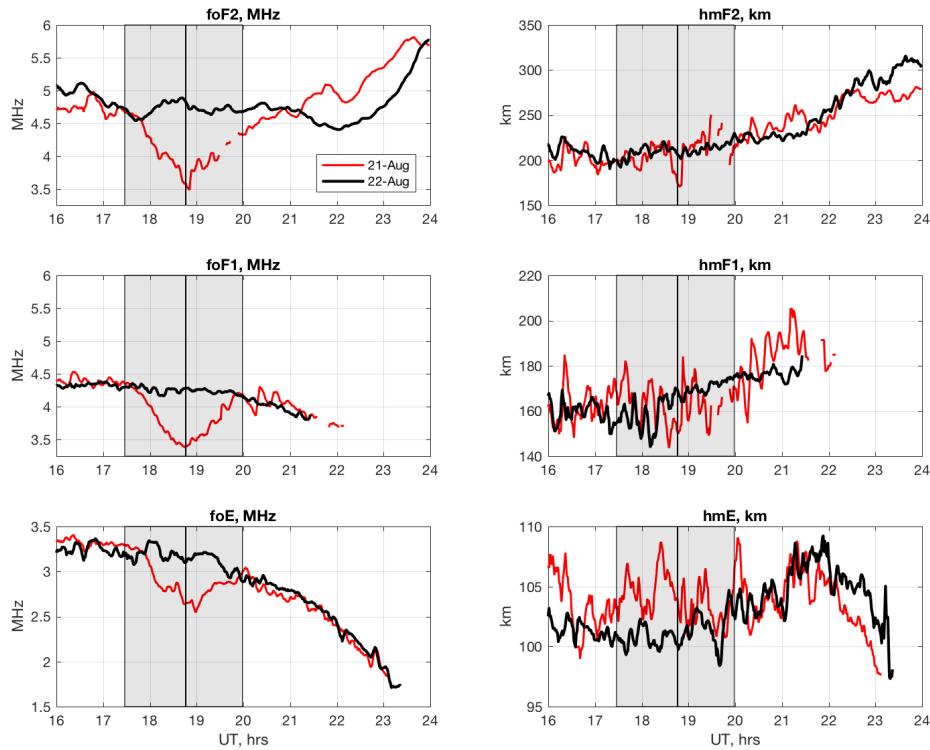
237 Upward plasma transport during daytime hours is typically a main source of plasma  
 238 to the mid-latitude plasmasphere where it can be stored for extended periods of time.  
 239 Consequently, we expect that topside electron density, initially depleted with eclipse onset,  
 240 was strongly increased during eclipse recovery following this enhanced upward motion.  
 241 We also suggest that a large post-eclipse disturbance in  $Ne$  observed in the evening hours,  
 242 21-24 UTC, is one of the primary effects of the eclipse. At 23-24 UT electron density in-  
 243 creased by  $> 50$ -120% around the peak of the F2-region, but decreased at higher altitudes,  
 244 as shown in Figure 3. This was also accompanied by a drop in electron and ion temper-  
 245 atures and a strong downward motion as seen in Figure 4. The plasmaspheric flux has a  
 246 generally positive non-eclipse trend in the daytime and negative at night at Millstone, with  
 247 a rapid increase observed at this seasonal point in the downward velocity of plasma af-  
 248 ter opposite hemisphere influence subsides due to conjugate sunset ( $\sim 23$  UTC). A sharp  
 249 onset of stronger downward vertical velocity and colder plasma temperature at 23 UT, to-  
 250 gether with an increase in  $Ne$  by  $>100\%$ , suggests that the local ionosphere was strongly  
 251 influenced by the downward influx of cold plasma with anomalously high density from  
 252 the plasmasphere reservoir, stored there by enhanced diffusive upward flux between 19-21



195 **Figure 4.** Difference in electron temperature (top), ion temperature (middle), and vertical plasma velocity  
 196 (bottom) observed on the eclipse day, August 21, 2017. August 22, 2017 is used as control day.

253 UTC as a result of the solar eclipse recovery. The question is whether such flux exchanges  
 254 at the topside ionosphere are efficient enough to impact electron density at ionospheric alti-  
 255 tudes. Dedicated simulation work as performed in [Reinisch et al, 2018] for the totality  
 256 zone can provide important insights.

257 Figure 5 compares digisonde observations of critical frequencies  $foF2$ ,  $foF1$ , and  
 258  $foE$  and peak heights  $hmF2$ ,  $hmF1$  and  $hmE$  during the eclipse day and control day Au-  
 259 gust 22. The main eclipse effect was a rapid decrease in  $foF2$ ,  $foF1$ , and  $foE$ , followed  
 260 by an enhanced post-eclipse  $foF2$  observed at 21-24 UTC. The magnitude of the eclipse-  
 261 induced decrease was close to 1 MHz in the  $F2$  region,  $\sim 0.7$  MHz in the  $F1$  region, and  
 262  $\sim 0.5$  MHz in the  $E$ -region. The start of the decreases occurred almost simultaneously at  
 263 different altitudes, contrary to earlier observations and simulations. The minimum frequen-  
 264 cies were observed with a 2-5 min lag after the maximum obscuration in the  $F2$  region  
 265 and very close to the maximum obscuration time at the  $F1$  region. The  $E$ -region response



234 **Figure 5.** Observations of peak critical frequencies and peak heights of  $F2$ ,  $F1$ , and  $E$  regions by Millstone  
 235 Hill digisonde on eclipse day August 21, 2017 and control day August 22, 2017. Shaded area indicates the  
 236 time of partial eclipse on August 21.

266 seems to have a longer delay than the  $F1$  region response. This is anomalous because,  
 267 from consideration of ionization and recombination processes, we expect the  $E$ -region to  
 268 respond faster to the eclipse,  $F1$  region with a short delay, and  $F2$  region with a longer  
 269 delay. We note that a C3 solar flare occurred between 17:39 and 17:57 UT, and anoma-  
 270 lous behavior described above could be related to the increase in the electron density due  
 271 to the flare. The timing of the variations observed in the digisonde data also might indi-  
 272 cate the presence of strong oscillations in electron density that are superimposed on the  
 273 eclipse response. In fact, observations of  $hmF2$ ,  $hmF1$ , and  $hmE$  indicate such oscillations  
 274 at all altitudes (Figure 5, right panels) and show that they were stronger on August 21,  
 275 2017, started prior to the eclipse, and thus could not be attributed entirely to the eclipse  
 276 effects. We will address the nature of these oscillations in a separate study.

## 277 5 Discussion and summary

278 This study examines mid-latitude ionospheric variations associated with the solar  
 279 eclipse on August 21, 2017 using both the Millstone Hill ISR and digisonde, at a location  
 280 more than 1000 km north-east from the center of totality and with maximum obscuration  
 281 63%. Here we summarize the most important features directly observed, some of which  
 282 present a challenge to current models of the coupled ionosphere and thermosphere.

- 283 1. The state of the ionosphere prior to the eclipse was significantly different than ex-  
 284 pected for this season and level of solar activity, based on a comparison with Mill-  
 285 stone Hill empirical model [Zhang and Holt, 2007]. The electron density was lower  
 286 by 20-40%, the electron temperature was elevated by 100-450 K, and the ion tem-  
 287 perature was decreased by 20-50 K. At least some of these differences were related  
 288 to the increase in geomagnetic activity for several days prior to the eclipse. In ad-  
 289 dition, we note the presence of oscillations in all ionospheric parameters with 2-3  
 290 hr periods and 20-60 minute periods that constitute typical ionospheric variabil-  
 291 ity and contribute additional 10-25% to variations. Anomalous conditions included  
 292 a very low (near or below 200 km) *F2* region peak height immediately preceding  
 293 the eclipse. This preconditioning is expected to influence ionospheric response to  
 294 the solar eclipse. In our quantitative estimates of eclipse effects, we account for all  
 295 these factors.
- 296 2. The 2017 eclipse caused a 30-40% decrease in electron density, 100-220 K de-  
 297 crease in electron temperature, and 50-140 K decrease in ion temperature. Contrary  
 298 to simulations [Roble et al, 1986; Ding et al, 2010] and prior observations, the  
 299 largest decrease in electron density was observed in the *F2* region, above 200 km,  
 300 and not in the *F1* region. This was consistent in observation by both instruments,  
 301 incoherent scatter radar and digisonde. The lowest electron density was observed  
 302 with a very short time lag after the maximum obscuration, 2-5 mins at 170-200 km  
 303 and 8-17 mins at  $\sim$ 240 km.
- 304 3. The eclipse-induced decrease in electron temperature reached 100-220 K, consider-  
 305 ably smaller than 450-1000 K decreases reported in earlier observations [Salah et  
 306 al, 1986; Chernyak and Lysenko, 2013] and simulations [Roble et al, 1986]. This  
 307 was possibly related to very low electron density prior to the eclipse and, conse-  
 308 quently, low electron cooling rates. The small  $T_e$  reduction was also consistent with  
 309 the large  $N_e$  reduction in the *F2* region stated above, as variations in these param-  
 310 eters are anti-correlated and heat content was maintained.
- 311 4. In contrast, the decrease in ion temperature during the eclipse reached 100-140 K  
 312 and was significantly higher than a  $\sim$ 55 K cooling expected from earlier simula-  
 313 tions for an eclipse with an even larger solar obscuration rate of 83% [Roble et al,  
 314 1986].
- 315 5. The most striking observation was a large 20-40 m/s upward plasma drift observed  
 316 above the *F2* region peak after the maximum obscuration. This upward plasma ve-  
 317 locity is similar to effects regularly observed after local sunrise due to associated  
 318 rapid increases in ionospheric and thermospheric temperature and resulting thermal  
 319 expansion. To the best of our knowledge, this is the first observational report of  
 320 eclipse-induced upward transport, as earlier studies reported only downward verti-  
 321 cal motion due to the thermospheric cooling. The simulation of Roble et al [1986]  
 322 indicated a small 2 m/s vertical drift during the eclipse recovery and in a narrow  
 323 300-400 km altitude range.
- 324 6. A strong upward vertical drift in the topside ionosphere was observed at 19-21 UT,  
 325 implying an anomalously high upward field aligned diffusion with associated re-  
 326 supply of topside electron density during the daytime hours and subsequent higher  
 327 downward plasmaspheric flux at nighttime. We hypothesize that a large enhance-  
 328 ment in the electron density observed at 21-24 UT as an important eclipse related  
 329 effect for the August 2017 event.

### 330 Acknowledgments

331 Millstone Hill operations and research at MIT Haystack Observatory are supported by co-  
 332 operative agreement AGS-1242204 between the US National Science Foundation and the  
 333 Massachusetts Institute of Technology. For eclipse activities, MIT Haystack was partially  
 334 supported by NASA grant NNX17AH71G. Millstone Hill ISR data is publicly available

335 through the Madrigal database at <http://madrigal.haystack.mit.edu/madrigal/>. Manually  
336 scaled digisonde data is available by request from I. Galkin.

## 337 References

- 338 Cherniak, I. and Lysenko, V., 2013. Measurements of the ionosphere plasma electron den-  
339 sity variation by the Kharkov incoherent scatter radar. *Acta Geophysica*, 61(5), pp.1289-  
340 1303.
- 341 Cherniak, I., & Zakharenkova, I. (2018). Ionospheric total electron content response to  
342 the great American solar eclipse of 21 August 2017. *Geophysical Research Letters*, 45.  
343 <https://doi.org/10.1002/2017GL075989>.
- 344 Ding F., W. Wan, B. Ning, L. Liu, H. Le, G. Xu, M. Wang, G. Li, Y. Chen, Z. Ren, B.  
345 Xiong, L. Hu, X. Yue, B. Zhao, F. Li, and M. Yang (2010), GPS TEC response to the  
346 22 July 2009 total solar eclipse in East Asia, *J. Geophys. Res.*, 2010, 115, A07308.
- 347 Domin, I.F., Yemel'yanov, L.Y., Kotov, D.V., Lyashenko, M.V. and Chernogor, L.F.,  
348 2013. Solar eclipse of August 1, 2008, above Kharkov: 1. Results of incoherent scat-  
349 ter observations. *Geomagnetism and Aeronomy*, 53(1), p.113.
- 350 Evans, J.V., 1965. An F region eclipse. *Journal of Geophysical Research*, 70(1), pp.131-  
351 142.
- 352 Evans, J.V., 1971. Observation of F region vertical velocities at Millstone Hill, 1, Evi-  
353 dence for drifts due to expansion, contraction, and winds. *Radio Science*, 6(6), pp.609-  
354 626.
- 355 Harding B. J., D. P. Drob, R. A. Buriti, J. J. Makela, (2018), Nightside detection of a  
356 large-scale thermospheric wave generated by a solar eclipse, *Geophysical Research Let-*  
357 *ters*, doi: 10.1002/2018GL077015.
- 358 Le, H., Liu, L., Yue, X. and Wan, W., 2008, The ionospheric responses to the 11 August  
359 1999 solar eclipse: observations and modeling. In *Annales Geophysicae* (Vol. 26, No. 1,  
360 pp. 107-116). Copernicus GmbH.
- 361 Muller-Wodarg, I. C. F., A. D. Aylward, and M. Lockwood (1998), Effects of a mid-  
362 latitude solar eclipse on the thermosphere and ionosphere - A modelling study, *Geo-*  
363 *phys. Res. Lett.*, 25(20), 3787-3790, doi:10.1029/1998GL900045.
- 364 Nayak, C. and Yiğit, E. (2017). GPS-TEC observation of gravity waves generated in the  
365 ionosphere during 21 August 2017 total solar eclipse. *Journal of Geophysical Research:*  
366 *Space Physics*, 122. <https://doi.org/10.1002/2017JA024845>
- 367 Reinisch, B. W., Dandenault, P. B., Galkin, I. A., Hamel, R., Richards, P. G. (2018), In-  
368 vestigation of the electron density variation during the 21 August 2017 solar eclipse.  
369 *Geophysical Research Letters*, 45, 1253-1261. <https://doi.org/10.1002/2017GL076572>
- 370 Roble, R.G., Emery, B.A. and Ridley, E.C., 1986. Ionospheric and thermospheric response  
371 over Millstone Hill to the May 30, 1984, annular solar eclipse. *Journal of Geophysical*  
372 *Research: Space Physics*, 91(A2), pp.1661-1670.
- 373 Salah, J. E., et al. (1986), Observations of the May 30, 1984, annular solar eclipse at Mill-  
374 stone Hill, *Journal of Geophysical Research: Space Physics* 91.A2 (1986): 1651-1660.
- 375 Savitzky, A., and Golay, M. J. E. (1964). Smoothing and differentiation of data by simpli-  
376 fied least squares procedures. *Analytical Chemistry*, 36, 1627-1639.
- 377 Wu, Chen, A. J. Ridley, L. Goncharenko, G. Chen, 2018. GITM-Data Comparisons of  
378 the Depletion and Enhancement during the 2017 Solar Eclipse. *Geophysical Research*  
379 *Letters*, doi: 10.1002/2018GL077409.
- 380 Zhang, S.R. and Holt, J.M., 2007. Ionospheric climatology and variability from long -  
381 term and multiple incoherent scatter radar observations: Climatology in eastern Ameri-  
382 can sector. *Journal of Geophysical Research: Space Physics*, 112(A6).

Figure1.

Author Manuscript

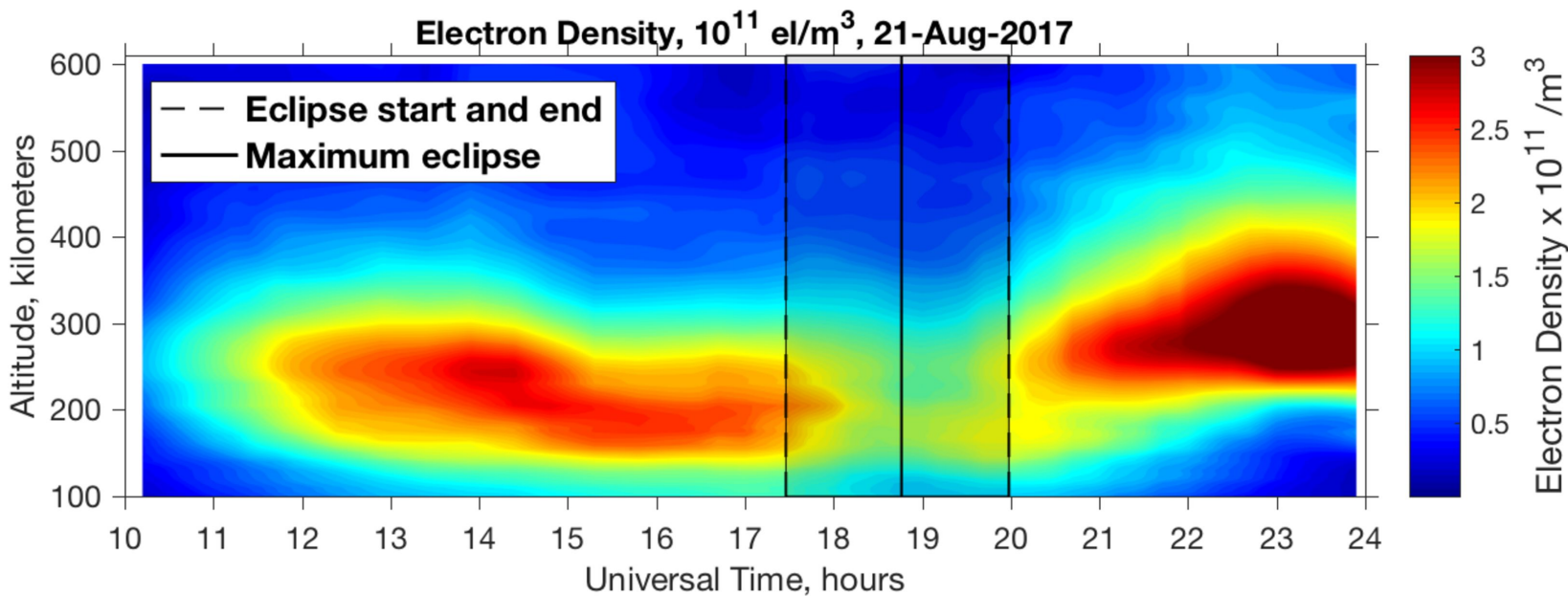
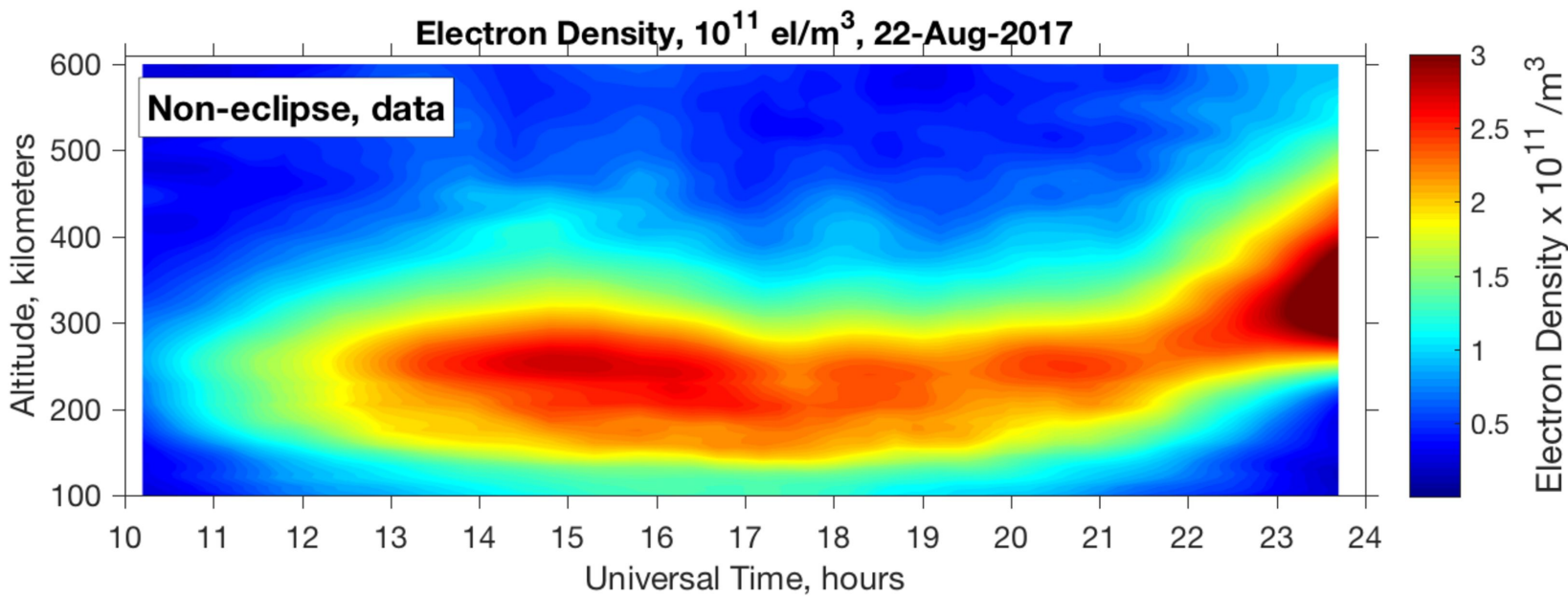
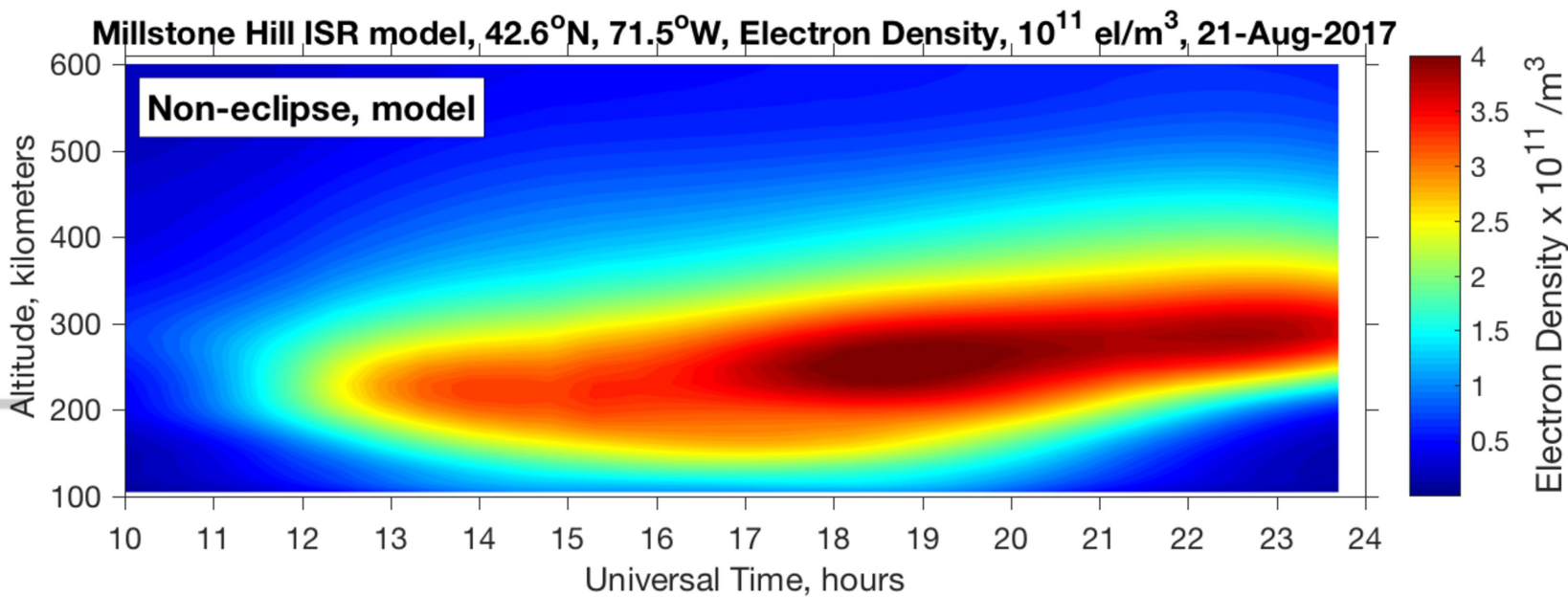
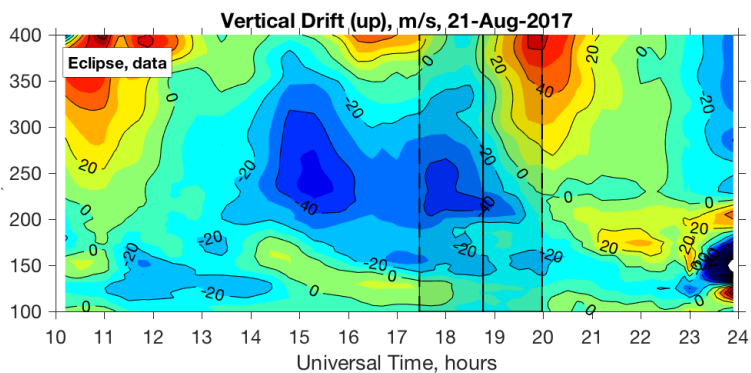
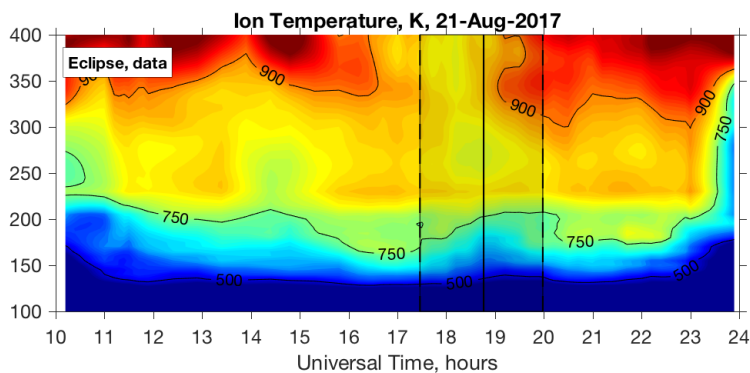
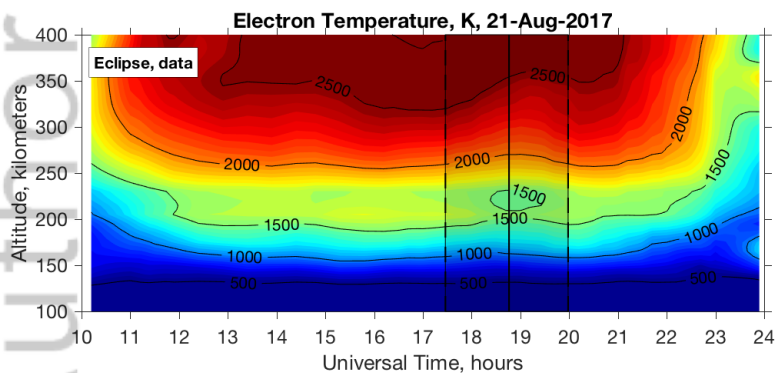
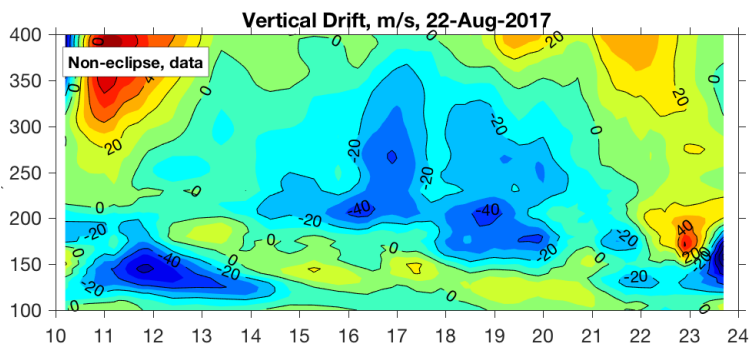
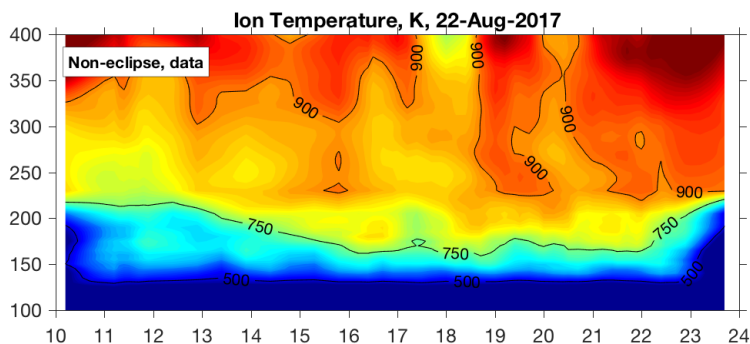
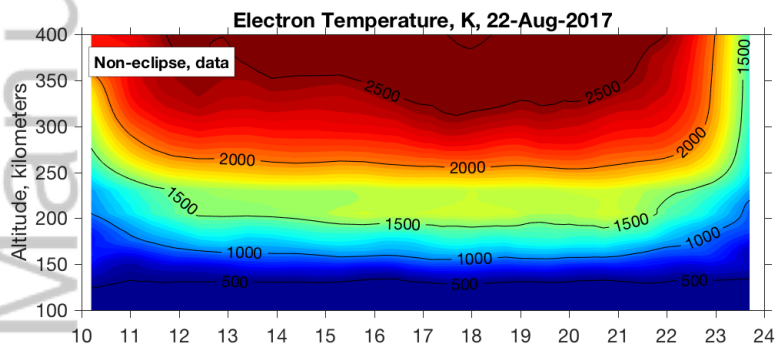
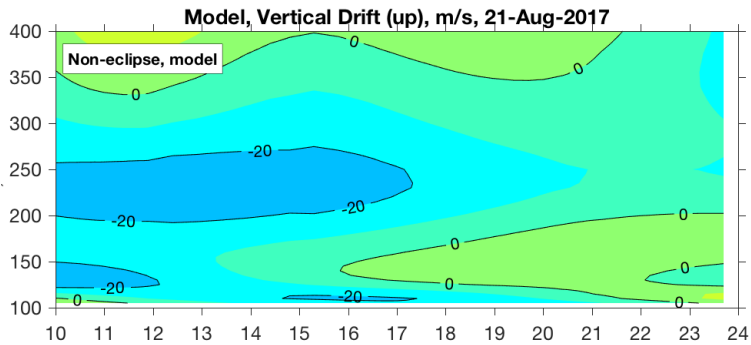
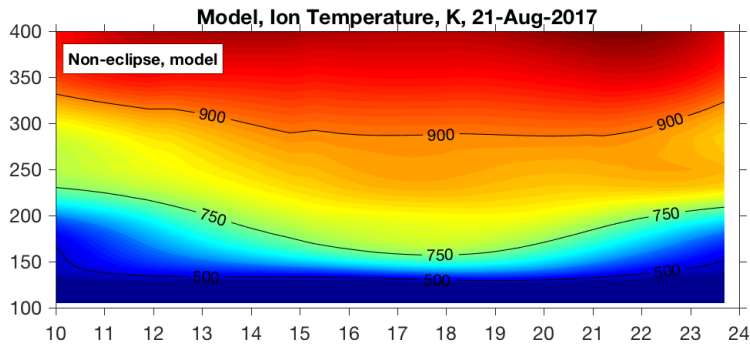
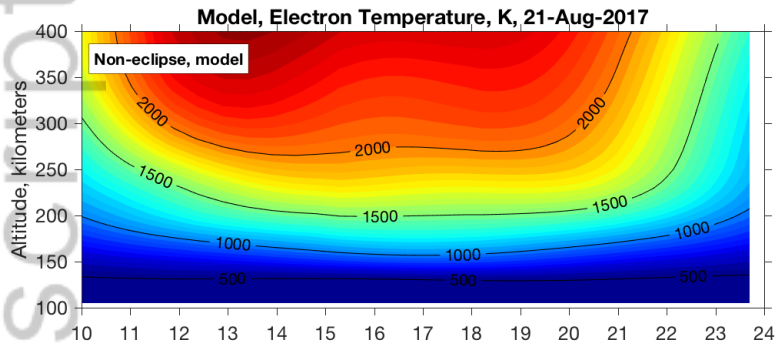


Figure2.

Author Manuscript



This article is protected by copyright. All rights reserved.

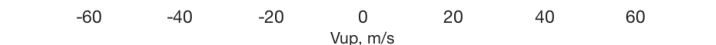
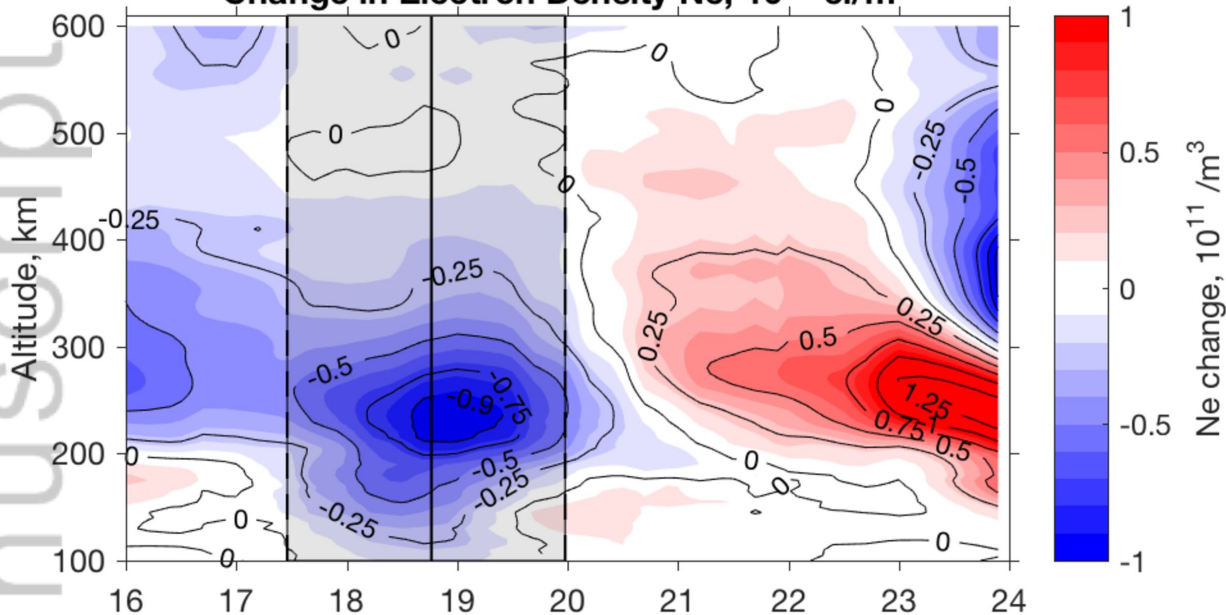


Figure3.

Author Manuscript

**Change in Electron Density  $N_e$ ,  $10^{11}$  el/m<sup>3</sup>**



**Change in Electron Density  $N_e$ , %**

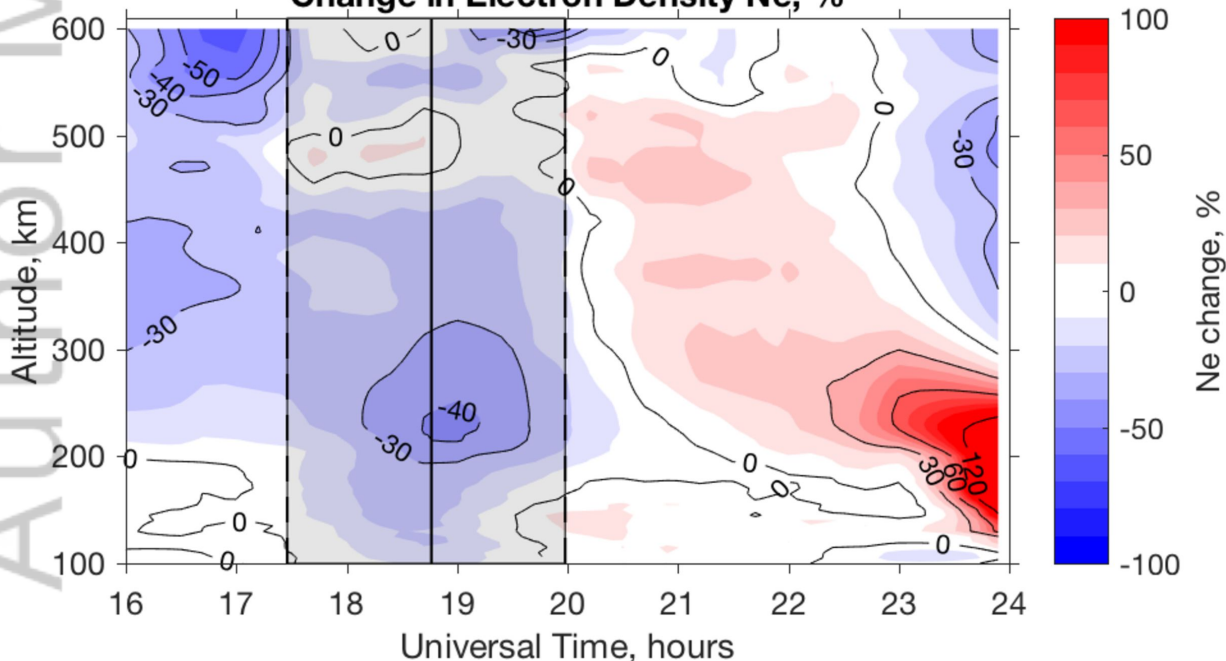


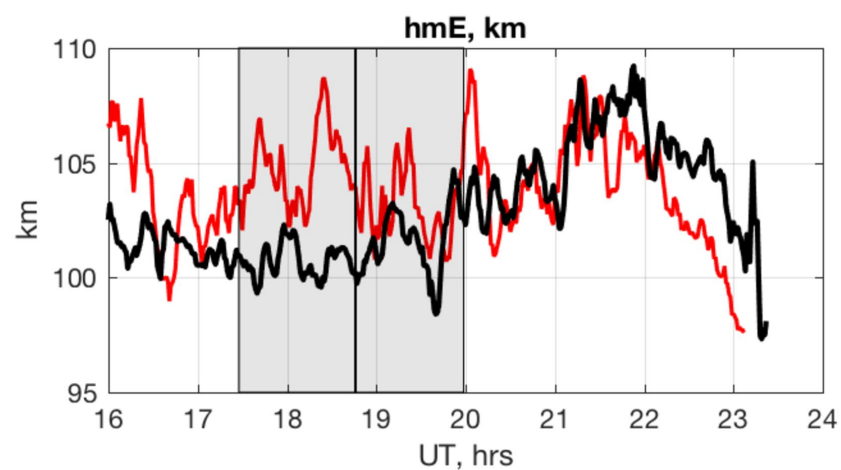
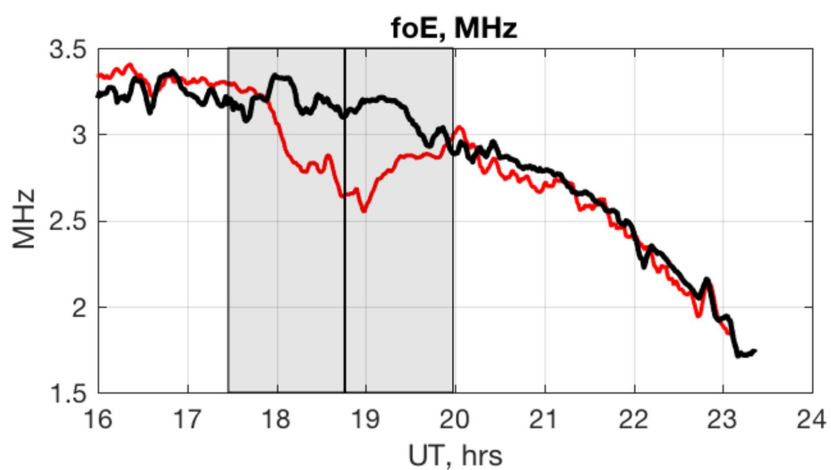
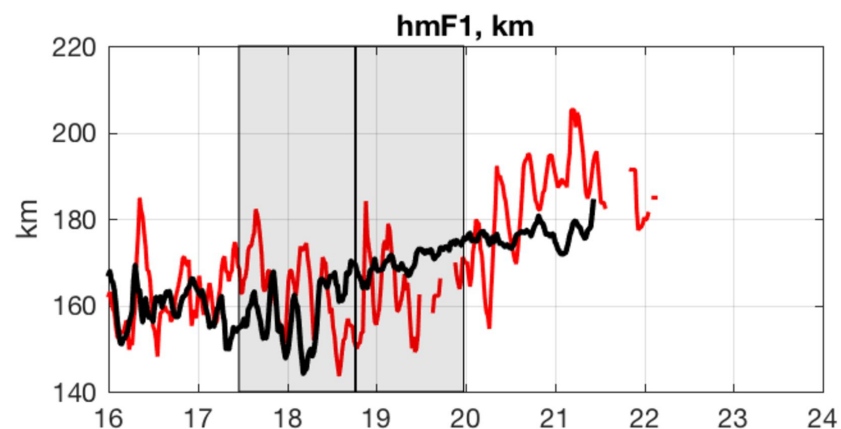
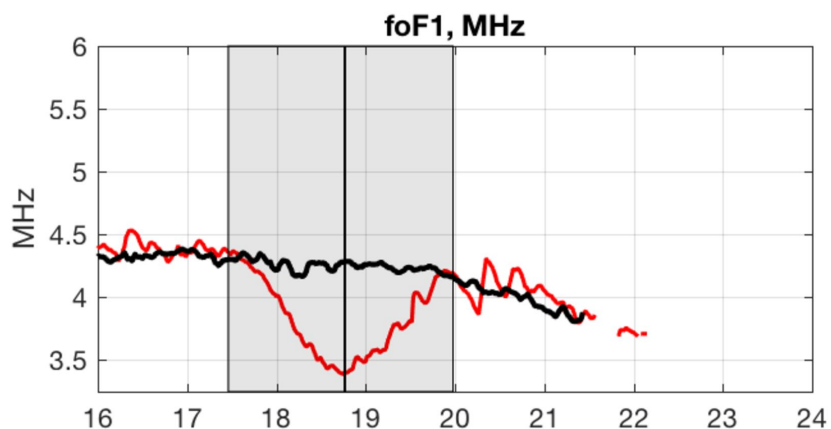
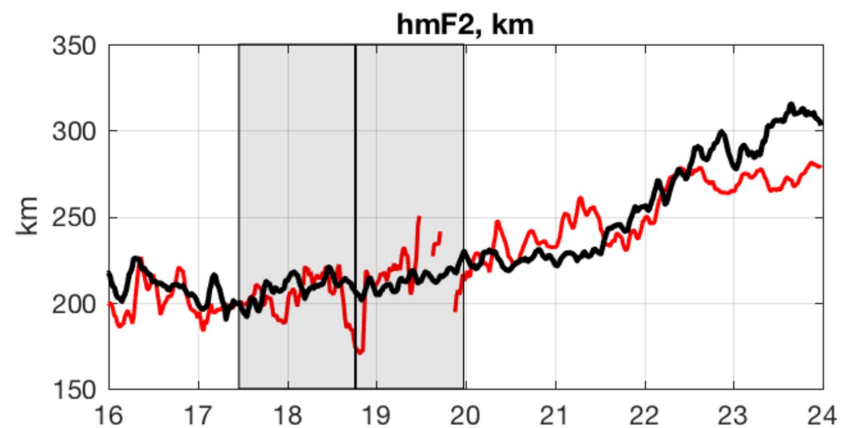
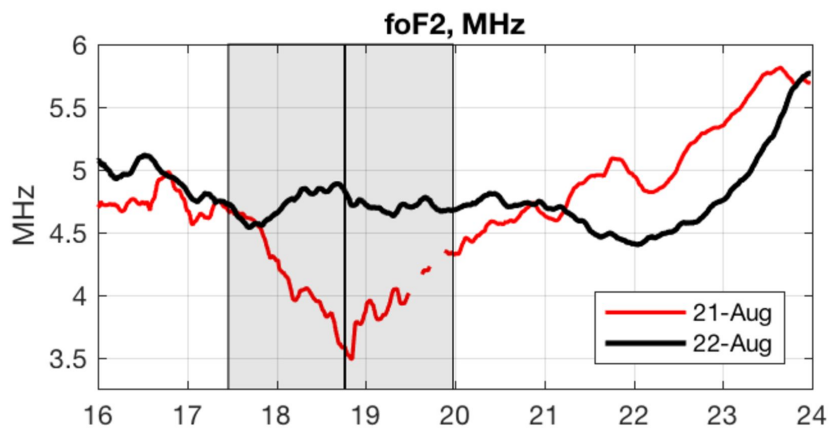
Figure4.

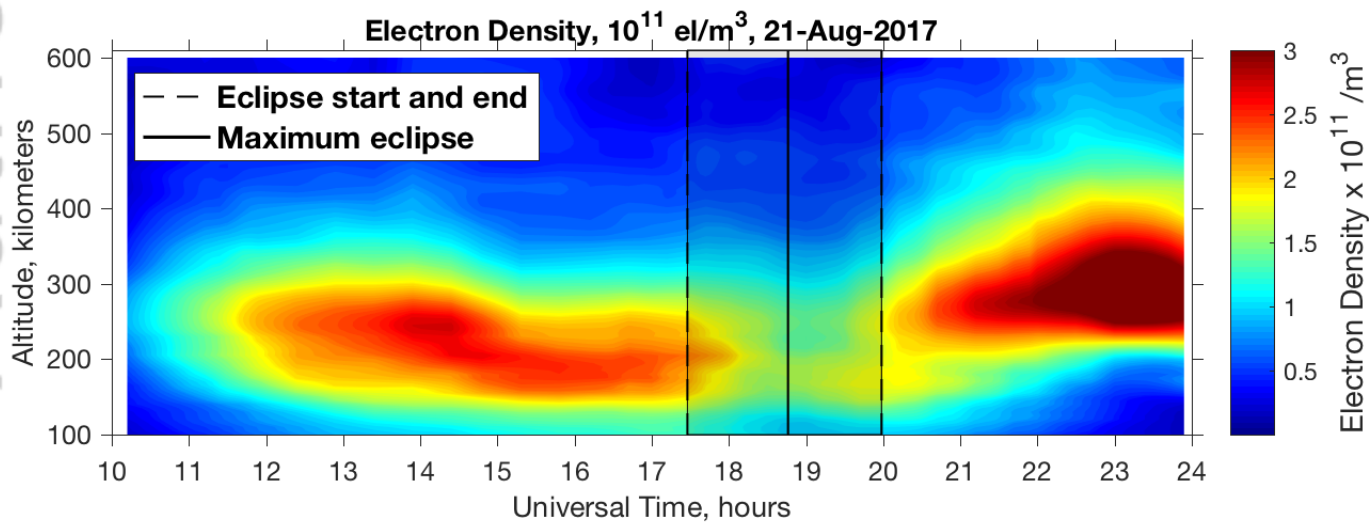
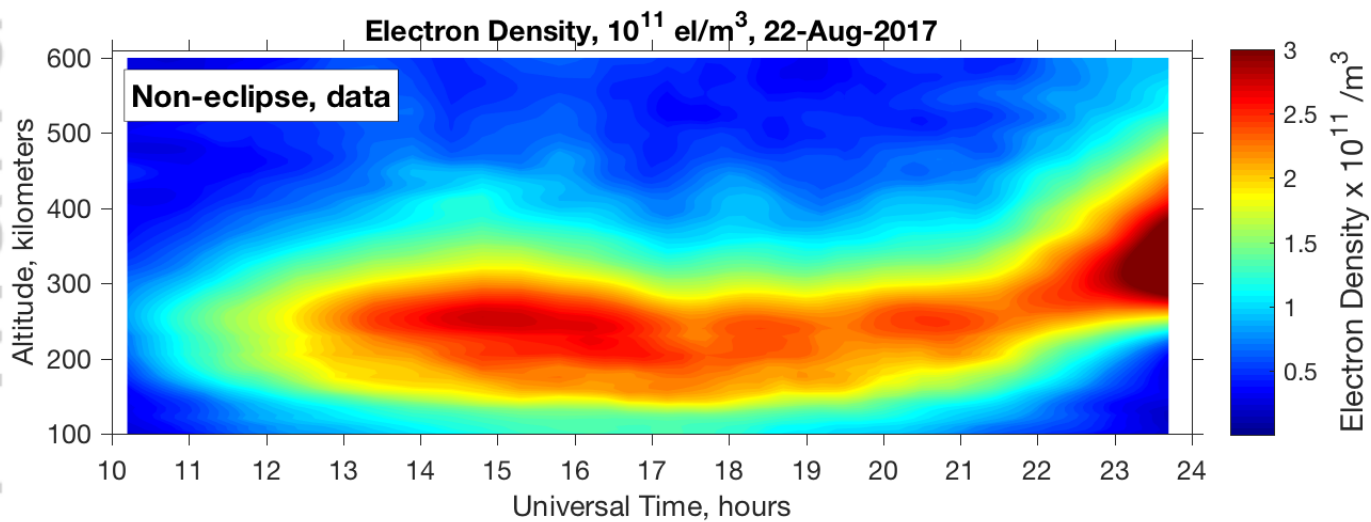
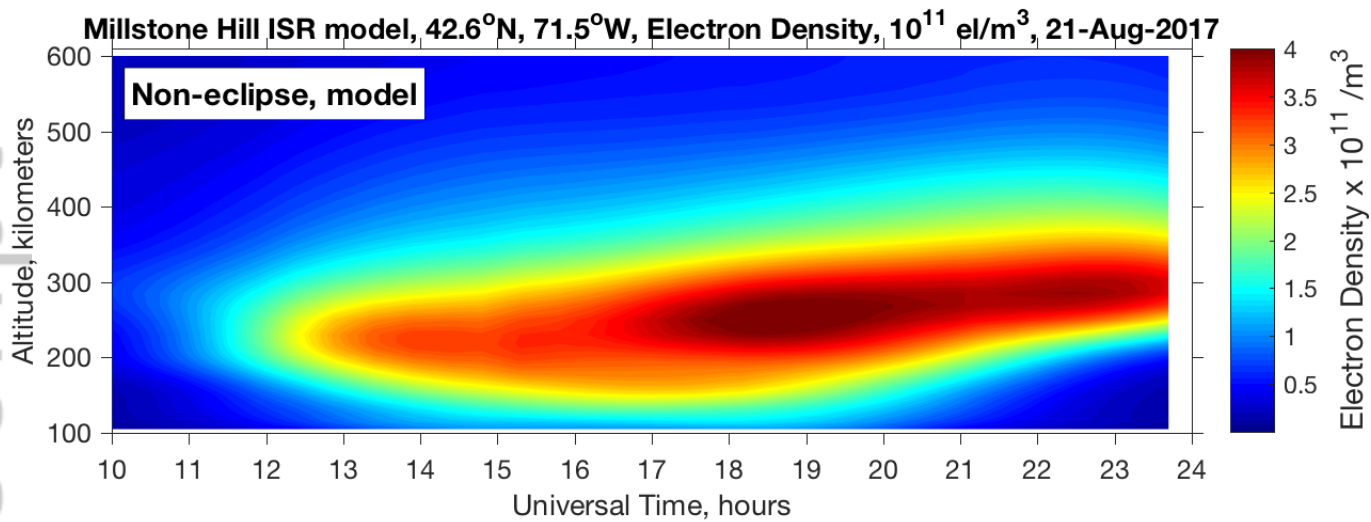
Author Manuscript



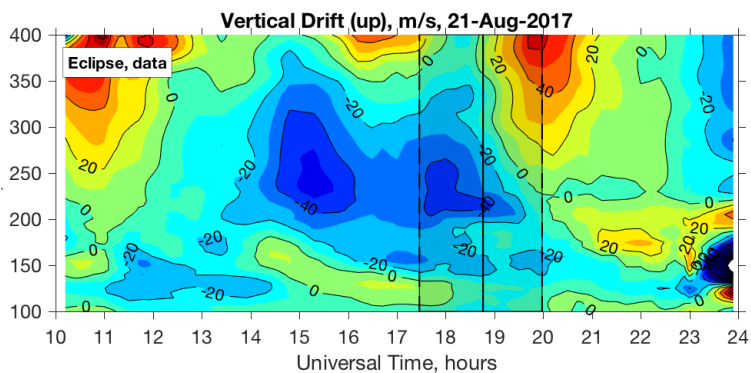
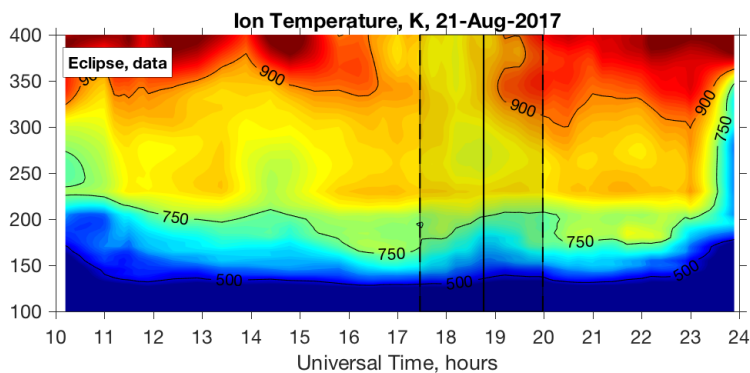
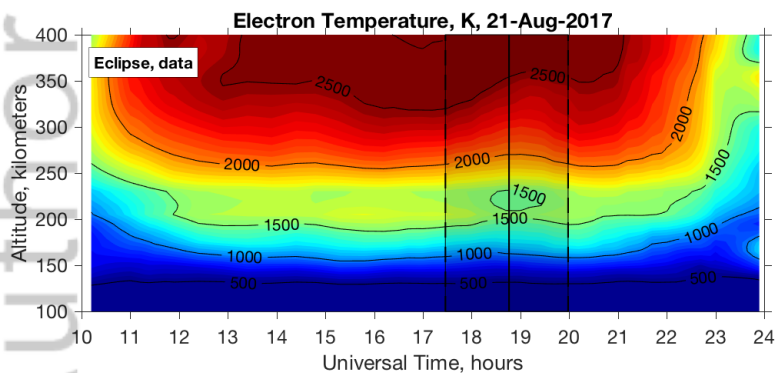
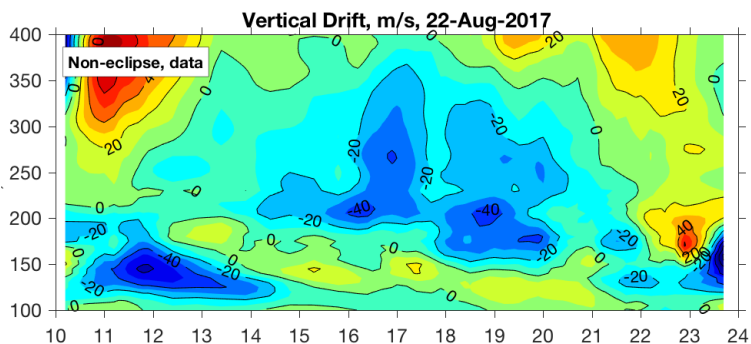
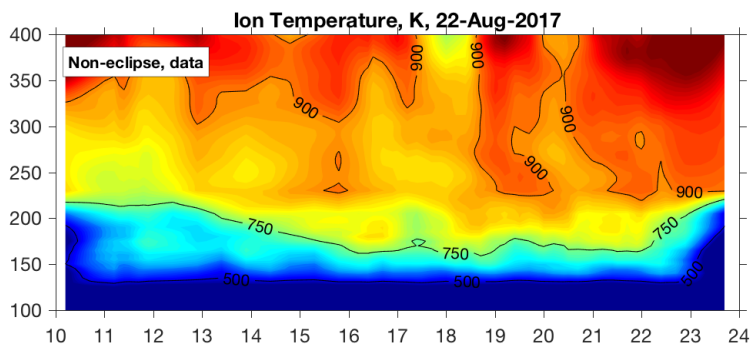
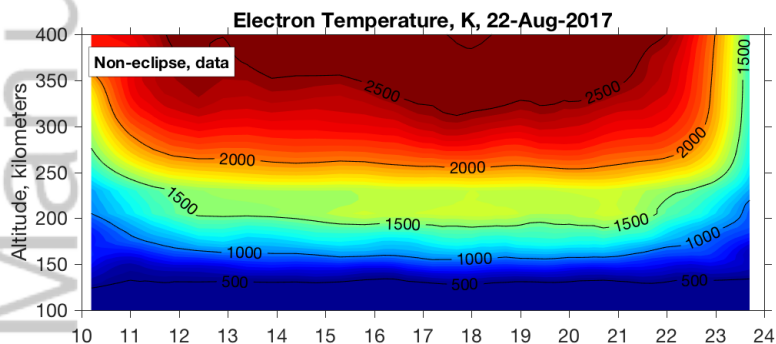
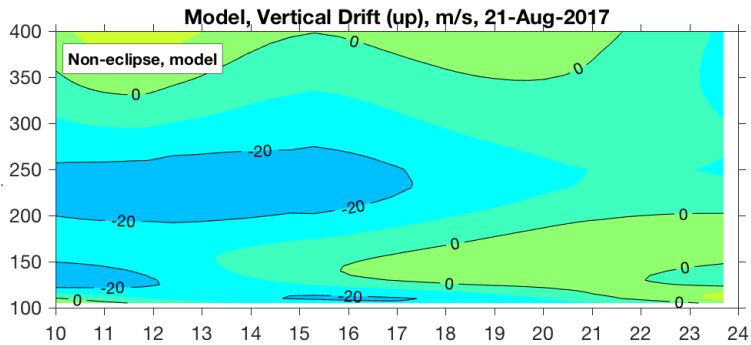
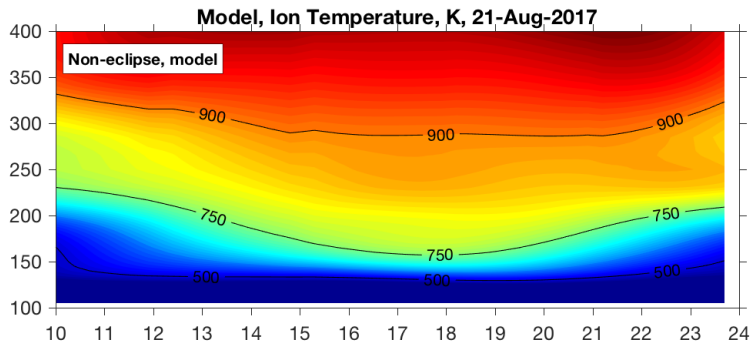
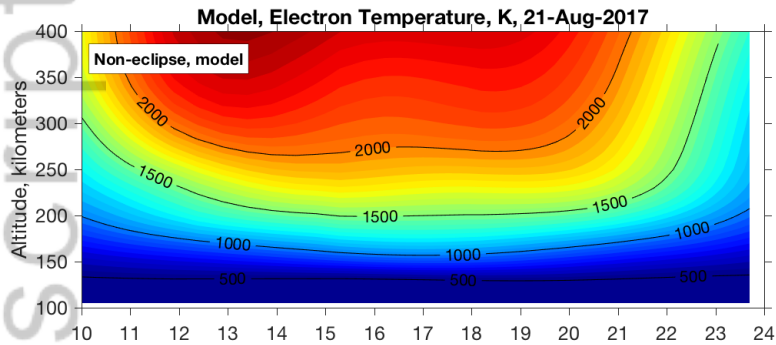
Figure5.

Author Manuscript

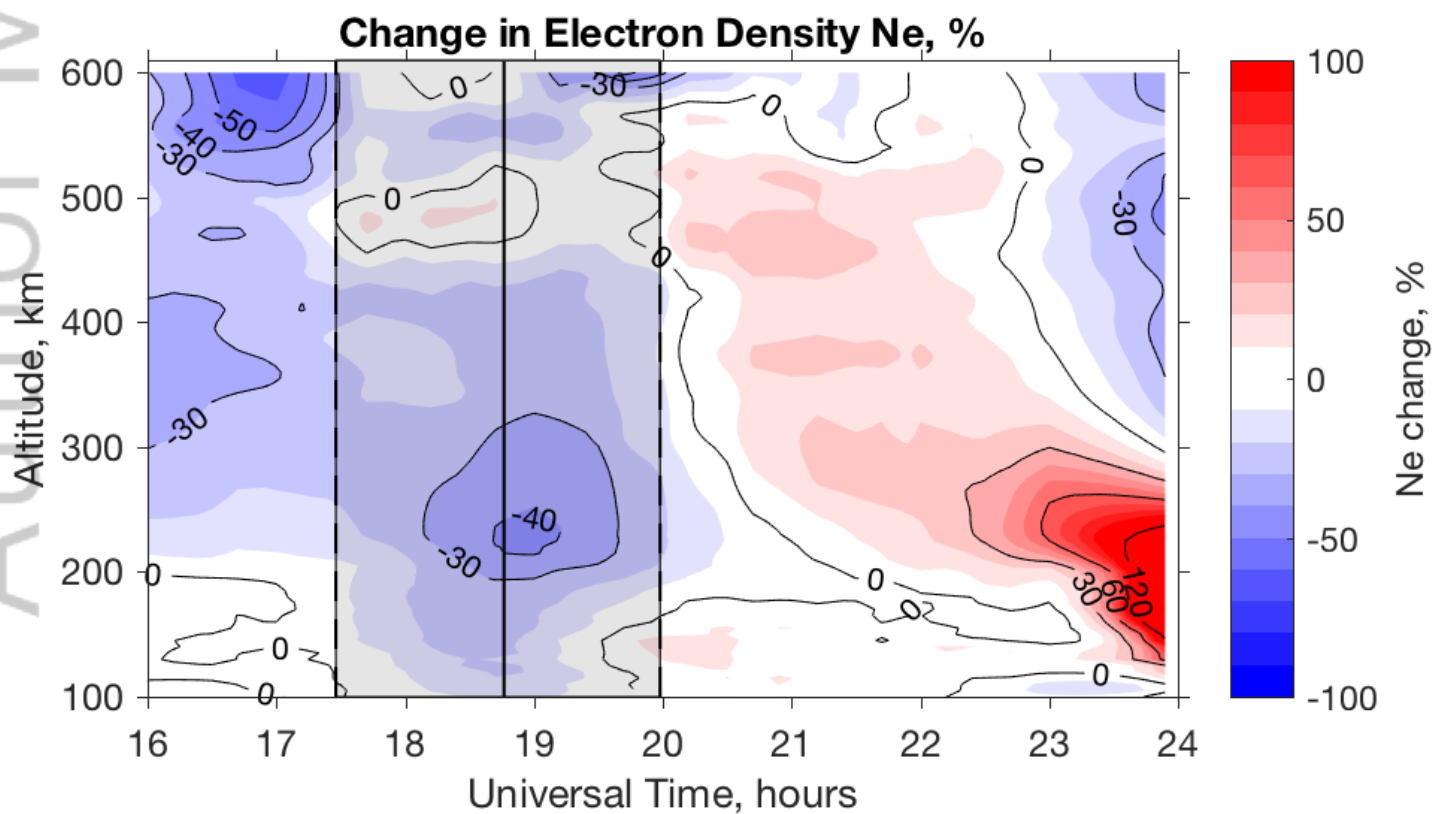
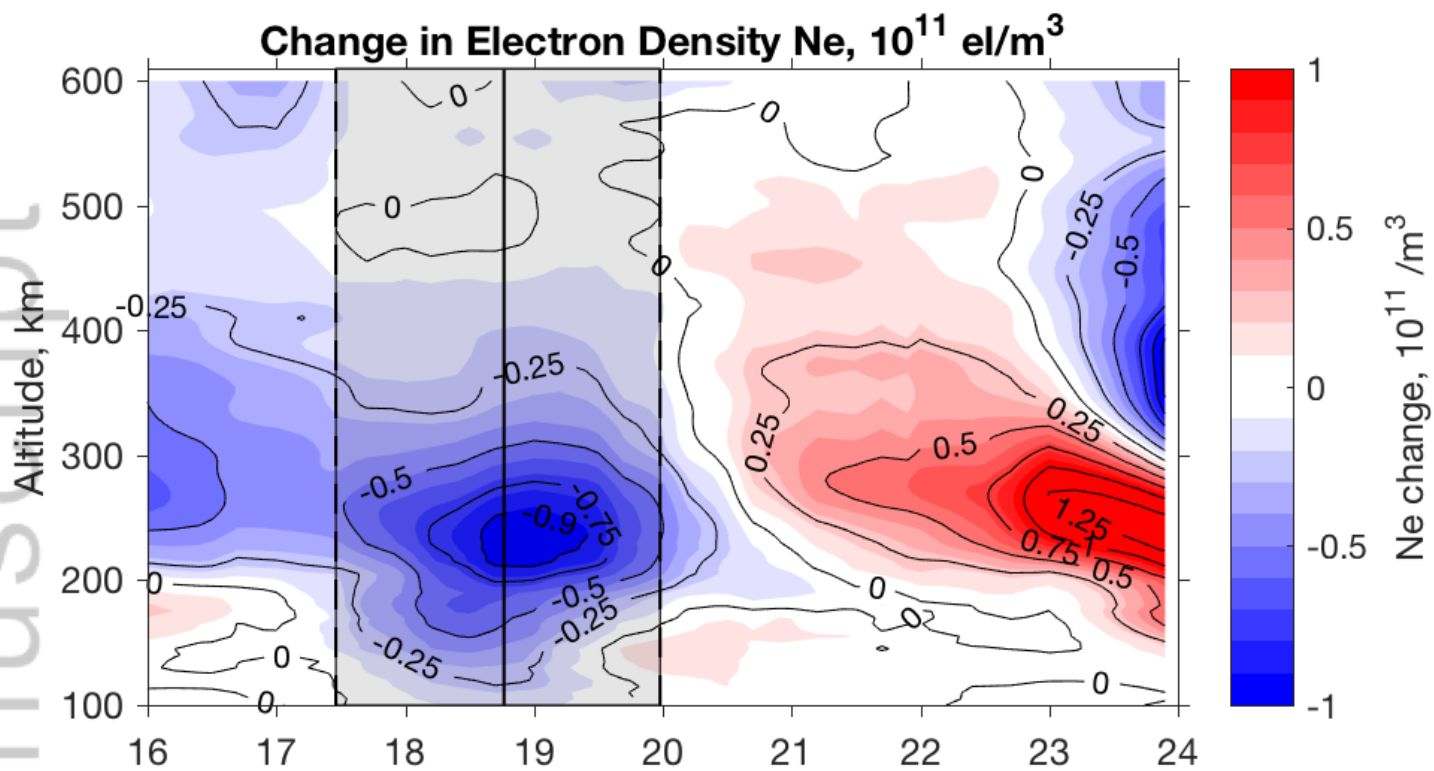


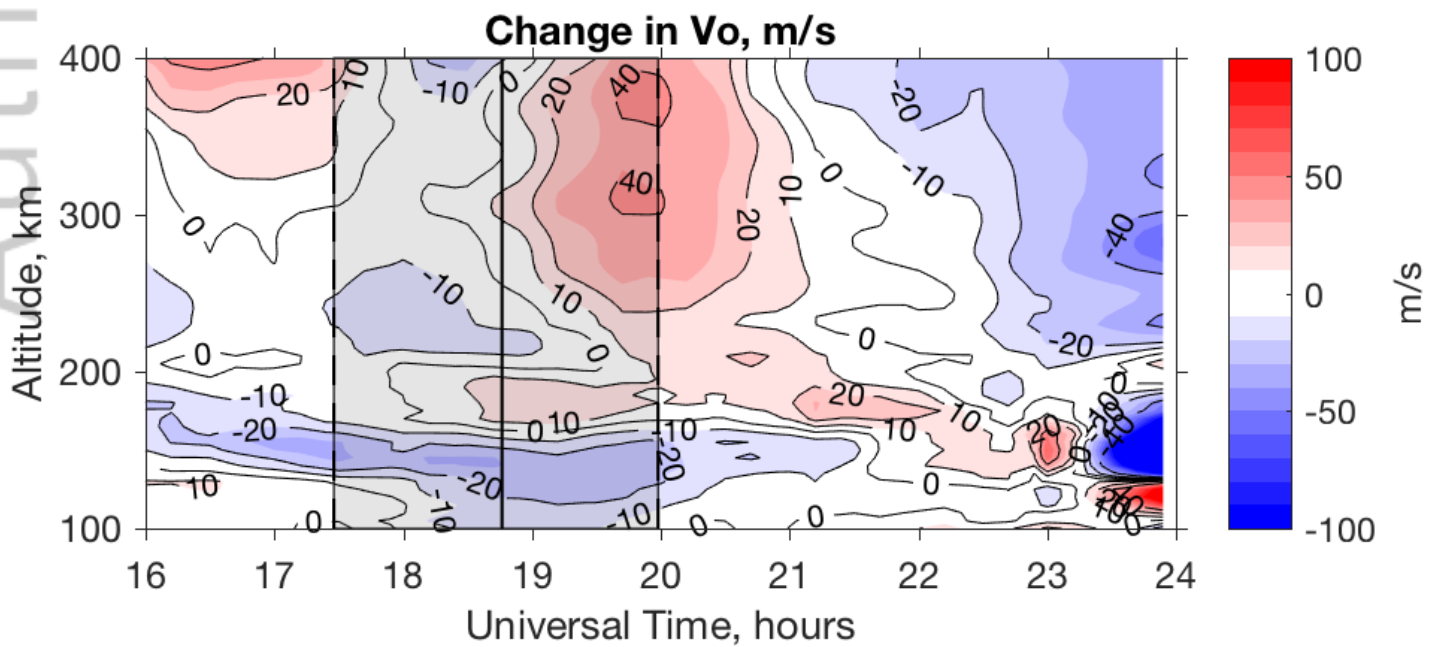
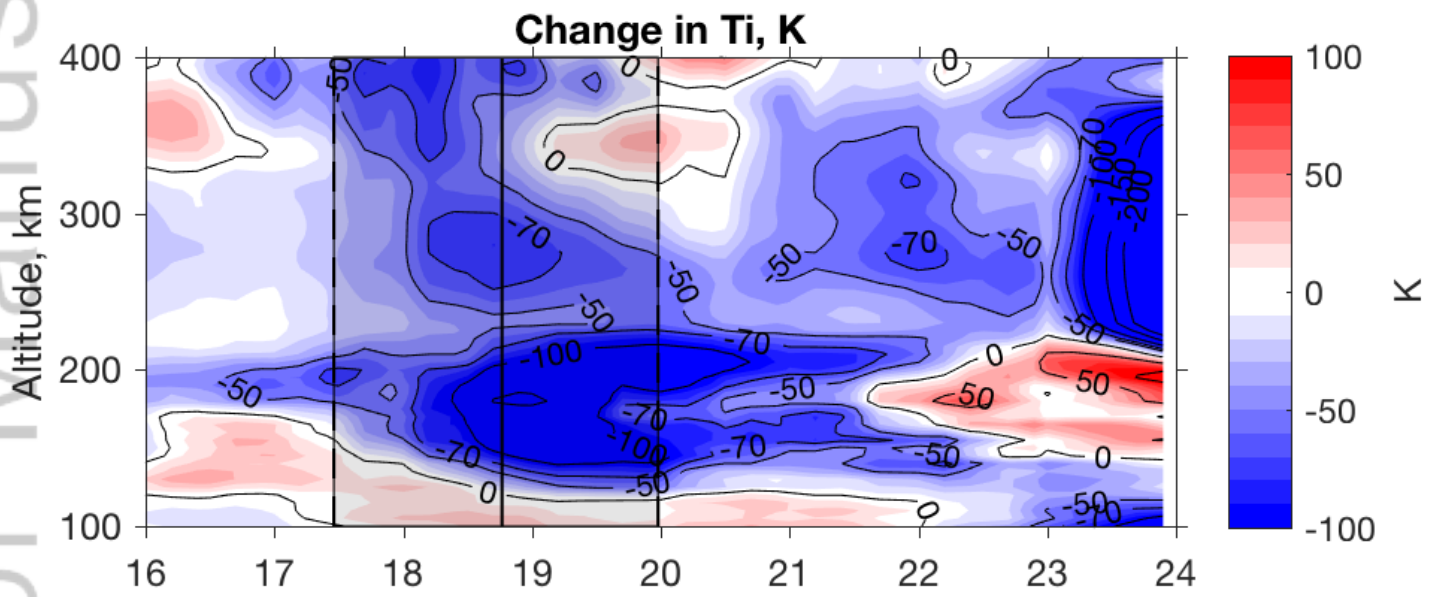
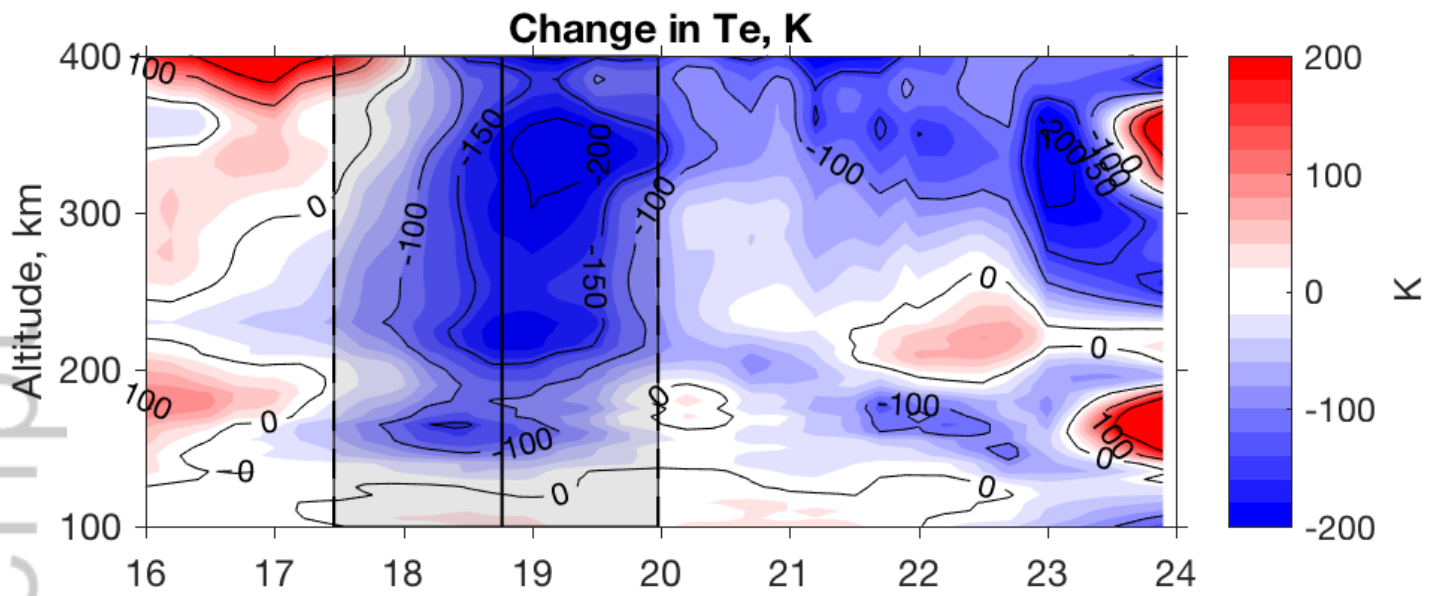


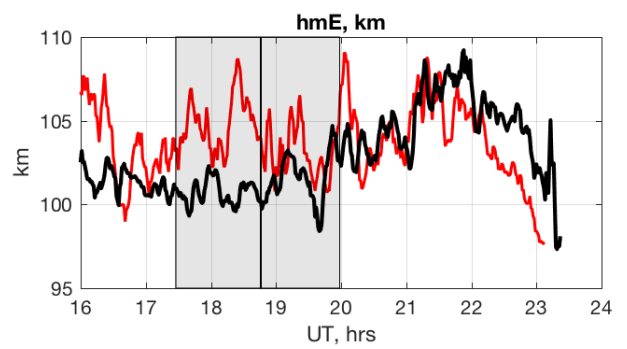
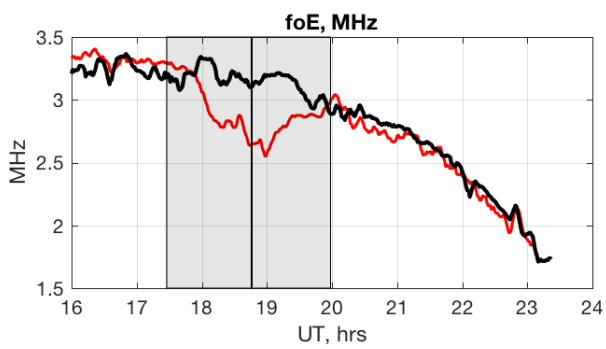
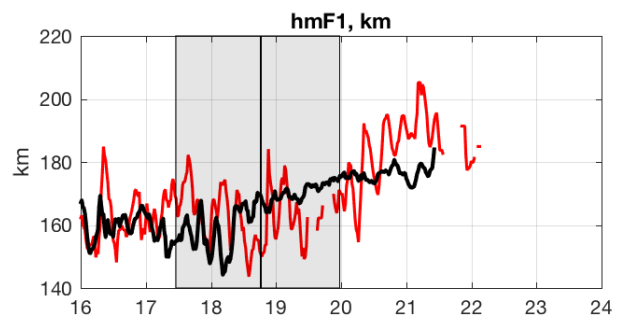
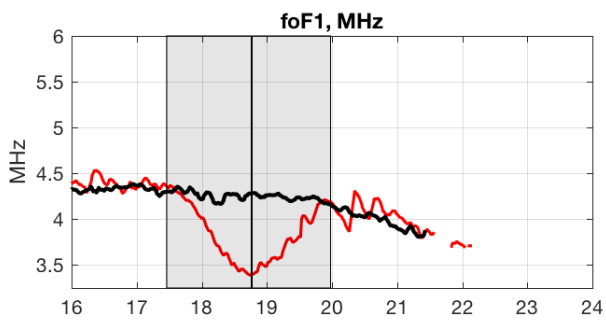
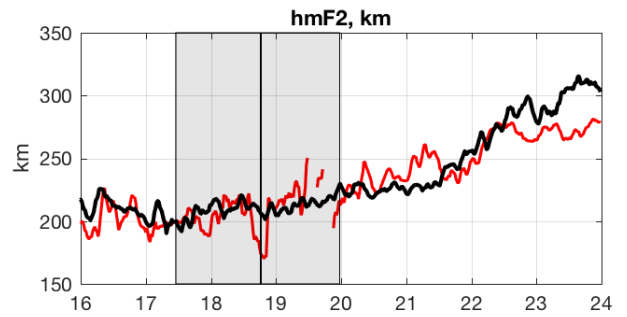
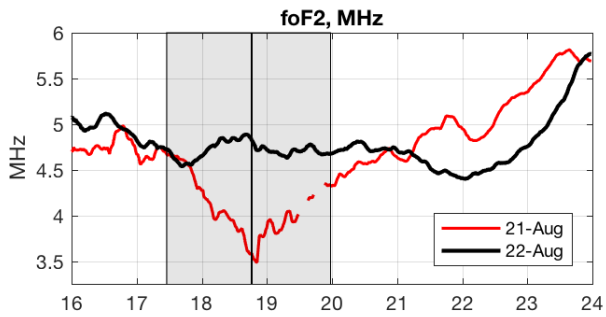
2018GL077334-f01-z.png



This article is protected by copyright. All rights reserved.







2018GL077334-f05-z-.png